Theoretical Physics

Multi-photon signatures at the Fermilab Tevatron

A.G. Akeroyd[1,a], A. Alves[2], M.A. Díaz[3], O. Éboli[2]

[1] Theory Group, KEK, 1-1 Oho, Tsukuba, 305-0801, Japan
[2] Instituto de Física, Universidade de São Paulo, São Paulo, Brazil
[3] Departamento de Física, Universidad Católica de Chile, Avenida Vicuña Mackenna 4860, Santiago, Chile

Abstract. Fermiophobic Higgs bosons ($h_{\rm f}$) exhibiting large branching ratios for decay to two photons can arise in models with two or more scalar doublets and/or triplets. In such models the conventional production mechanisms at hadron colliders, which rely on the $h_{\rm f}VV$ coupling ($V = W, Z$), may be rendered ineffective due to severe mixing angle suppression. In this scenario, double $h_{\rm f}$ production may proceed via the complementary mechanism $qq' \to H^{\pm}h_{\rm f}$ with subsequent decay $H^{\pm} \to h_{\rm f}W^*$, leading to events with up to four photons. We perform a simulation of the detection prospects of $h_{\rm f}$ in the multi-photon (> 3) channel at the Fermilab Tevatron and show that a sizeable region of the ($m_{H^{\pm}}, m_{h_{\rm f}}$) parameter space can be probed during Run II.

1 Introduction

Neutral Higgs bosons with very suppressed couplings to fermions – "fermiophobic Higgs bosons" ($h_{\rm f}$) [1] – may arise in specific versions of the two Higgs doublet model (2HDM) [2, 3] or in models with Higgs triplets [4, 5]. Such a $h_{\rm f}$ would decay dominantly to two photons, $h_{\rm f} \to \gamma\gamma$, for $m_{h_{\rm f}} < 95$ GeV or to two massive gauge bosons, $h_{\rm f} \to VV^{(*)}$, ($V = W^{\pm}, Z$) for $m_{h_{\rm f}} > 95$ GeV [6, 7]. The large branching ratio (BR) for $h_{\rm f} \to \gamma\gamma$ would provide a very clear experimental signature, and observation of such a particle would strongly constrain the possible choices of the underlying Higgs sector [6–12].

Experimental searches for $h_{\rm f}$ at LEP and the Fermilab Tevatron have been negative so far. Mass limits have been set in a benchmark model which assumes that the coupling $h_{\rm f}VV$ has the same strength as the standard model (SM) Higgs coupling $VV\phi^0$, and that all fermion BRs are exactly zero. Lower bounds of the order $m_{h_{\rm f}} \gtrsim 100$ GeV have been obtained by the LEP Collaborations OPAL [13], DELPHI [14, 15], ALEPH [16], and L3 [17, 18], utilizing the channel $e^+e^- \to h_{\rm f}Z$, $h_{\rm f} \to \gamma\gamma$. At the Tevatron Run I, the limits on $m_{h_{\rm f}}$ from the DØ and CDF Collaborations are respectively 78.5 GeV [19] and 82 GeV [20] at 95% C.L., using the mechanism $qq' \to V^* \to h_{\rm f}V$, $h_{\rm f} \to \gamma\gamma$, with the dominant contribution coming from $V = W^{\pm}$. For an integrated luminosity of $2 \,{\rm fb}^{-1}$, Run II will extend the coverage of $m_{h_{\rm f}}$ in the benchmark model slightly beyond that of

[a] e-mail: akeroyd@post.kek.jp

LEP [21, 23]. In addition, Run II will be sensitive to the region 110 GeV $< m_{h_{\rm f}} <$ 160 GeV and BR($h_{\rm f} \to \gamma\gamma$) $> 4\%$ which could not be probed at LEP. A preliminary search in the inclusive $2\gamma + X$ channel has been performed with $190 \,{\rm pb}^{-1}$ of Run II data [24].

However, the $h_{\rm f}VV$ coupling in a specific model could be suppressed relative to the ϕ^0VV coupling by a mixing angle, leading to a weakening of the above mass limits. If this suppression were quite severe ($h_{\rm f}VV/\phi^0VV < 0.1$) a very light $h_{\rm f}$ ($m_{h_{\rm f}} \ll 100$ GeV) would have eluded the searches at LEP and the Tevatron Run I in production mechanisms which rely upon the $h_{\rm f}VV$ coupling. Therefore it is of interest to consider other production mechanisms for $h_{\rm f}$ which may allow for observable rates if the $h_{\rm f}VV$ coupling is suppressed. Since the couplings $h_{\rm f}VV$ and $h_{\rm f}VH$ (where H is another Higgs boson in the model) are complementary, two LEP Collaborations, i.e. OPAL [13] and DELPHI [14, 15], also searched for fermiophobic Higgs bosons in the channel $e^+e^- \to A^0h_{\rm f}$, and ruled out the region $m_A + m_{h_{\rm f}} < 160$ GeV. However, a very light $m_{h_{\rm f}} < 50$ GeV is still possible if m_A is sufficiently heavy.

An alternative production mechanism which also depends on the complementary $h_{\rm f}VH$ coupling is the process $qq' \to H^{\pm}h_{\rm f}$ [25, 26]. Such a mechanism is exclusive to a hadron collider and can offer promising rates at the Tevatron Run II, provided that $H^{\pm}$ is not too far above its present mass bound $m_{H^{\pm}} > 90$ GeV. This alternative experimental signature depends on the decays of $H^{\pm}$. In fermiophobic models the decay $H^{\pm} \to h_{\rm f}W^{(*)}$ can have a larger BR than the conventional decays $H^{\pm} \to tb, \tau\nu$ [27, 28], which leads to double $h_{\rm f}$ production.

In this paper we analyze the inclusive production of multi-photon (3γ's or 4γ's) final states at the Tevatron RUN II via the mechanism

$$p\bar{p} \to h_{\mathrm{f}}H^{\pm} \to h_{\mathrm{f}}h_{\mathrm{f}}W^{\pm} \to \gamma\gamma\gamma(\gamma) + X \,.$$

In the 2HDM the multi-photon signature arises in the parameter space $m_{h_{\mathrm{f}}} \lesssim 90$ GeV, $m_{H^{\pm}} \lesssim 200$ GeV, and $\tan\beta > 1$. In this region, $\mathrm{BR}(h_{\mathrm{f}} \to \gamma\gamma) \sim 1$ and $\mathrm{BR}(H^{\pm} \to h_{\mathrm{f}}W^{*\pm}) \sim 1$, leading to a 4γ + leptons or jets signature. The multi-photon signature has the added virtue of being extremely clean concerning the background contamination, in contrast to the conventional searches for single h_{f} production in the channels $\gamma\gamma + V$ and $\gamma\gamma + X$. In the present work we show that the multi-photon signal can be observed in a large fraction of the $m_{h_{\mathrm{f}}} \otimes m_{H^{\pm}}$ plane at the Tevatron RUN II. In fact, at 3σ level of statistical significance, the RUN II will be able to exclude Higgs masses up to $m_{H^{\pm}} \lesssim 240$ GeV for very light $m_{h_{\mathrm{f}}}$, or $m_{h_{\mathrm{f}}} \lesssim 100$ GeV for $m_{H^{\pm}} \approx 100$ GeV.

Our work is organized as follows. In Sect. 2 we give a brief introduction to fermiophobic Higgs bosons, exhibiting the main decay channels of h_{f} and $H^{\pm}$. The possible fermiophobic Higgs production mechanisms and respective signatures are described in Sect. 3. We present our analyses in Sect. 4, and Sect. 5 contains our conclusions.

2 Fermiophobic Higgs bosons

In this section we briefly review the properties of h_{f}. For a detailed introduction we refer the reader to [7,10–12]. Fermiophobia can arise in (i) 2HDM (Model I) and (ii) Higgs triplets models.

In (i) the imposition of a discrete symmetry together with a vanishing mixing angle ensures exact fermiophobia at tree level. In (ii), gauge invariance forbids any coupling of h_{f} to quarks while lepton couplings are strongly constrained by neutrino oscillation data and lepton flavor violation experiments, resulting in approximate fermiophobia at tree level.

2.1 2HDM (Model I)

If Φ_1 and Φ_2 are two Higgs $SU(2)$ doublets with hypercharge $Y = 1$, the most general $SU(2) \times U(1)$ gauge invariant scalar potential is [29]

$$\begin{aligned} V =\ & m_{11}^2 \Phi_1^{\dagger}\Phi_1 + m_{22}^2 \Phi_2^{\dagger}\Phi_2 - \left(m_{12}^2 \Phi_1^{\dagger}\Phi_2 + \mathrm{h.c.} \right) \\ & + \tfrac{1}{2}\lambda_1 \left(\Phi_1^{\dagger}\Phi_1 \right)^2 + \tfrac{1}{2}\lambda_2 \left(\Phi_2^{\dagger}\Phi_2 \right)^2 + \lambda_3 \left(\Phi_1^{\dagger}\Phi_1 \right)\left(\Phi_2^{\dagger}\Phi_2 \right) \\ & + \lambda_4 \left(\Phi_1^{\dagger}\Phi_2 \right)\left(\Phi_2^{\dagger}\Phi_1 \right) + \left\{ \tfrac{1}{2}\lambda_5 \left(\Phi_1^{\dagger}\Phi_2 \right)^2 \right. \\ & \left. + \left[\lambda_6 \left(\Phi_1^{\dagger}\Phi_1 \right) + \lambda_7 \left(\Phi_2^{\dagger}\Phi_2 \right) \right] \Phi_1^{\dagger}\Phi_2 + \mathrm{h.c.} \right\} \,. \end{aligned} \tag{1}$$

If the discrete symmetry $\Phi_1 \to -\Phi_1$ is imposed, the couplings obey $\lambda_6 = \lambda_7 = 0$. However, the term proportional to m_{12}^2 can remain as a soft violation of the above discrete symmetry and still ensure that Higgs-mediated tree-level flavor changing neutral currents are absent [3]. Note that the above 2HDM potential contains one more free parameter than those studied in [11,12].

The potential in (1) breaks $\mathrm{SU}(2)_{\mathrm{L}} \times \mathrm{U}(1)_Y$ down to $\mathrm{U}(1)_{\mathrm{em}}$ when the two Higgs doublets acquire vacuum expectation values

$$\langle \Phi_1 \rangle = \frac{1}{\sqrt{2}} \begin{pmatrix} 0 \\ v_1 \end{pmatrix}, \qquad \langle \Phi_2 \rangle = \frac{1}{\sqrt{2}} \begin{pmatrix} 0 \\ v_2 \end{pmatrix}, \tag{2}$$

which must satisfy the experimental constraint $m_Z^2 = \frac{1}{2}(g^2 + g'^2)(v_1^2 + v_2^2) \approx (91 \text{ GeV})^2$. The minimization conditions that define the vacuum expectation values in terms of the parameters of the potential ($\lambda_6 = \lambda_7 = 0$) are

$$\begin{aligned} t_1 &= m_{11}^2 v_1 - m_{12}^2 v_2 + \tfrac{1}{2}\lambda_1 v_1^3 + \tfrac{1}{2}(\lambda_3 + \lambda_4 + \lambda_5)v_1 v_2^2 = 0, \\ t_2 &= m_{22}^2 v_2 - m_{12}^2 v_1 + \tfrac{1}{2}\lambda_2 v_2^3 + \tfrac{1}{2}(\lambda_3 + \lambda_4 + \lambda_5)v_1^2 v_2 = 0, \end{aligned} \tag{3}$$

from which m_{11}^2 and m_{22}^2 can be solved in favor of m_Z^2 and $\tan\beta \equiv v_2/v_1$.

The neutral CP-odd Higgs mass matrix is, after using the minimization conditions,

$$\mathbf{M}_A^2 = \begin{pmatrix} m_{12}^2 t_{\beta} - \lambda_5 v^2 s_{\beta}^2 & -m_{12}^2 + \lambda_5 v^2 s_{\beta}c_{\beta} \\ -m_{12}^2 + \lambda_5 v^2 s_{\beta}c_{\beta} & m_{12}^2/t_{\beta} - \lambda_5 v^2 c_{\beta}^2 \end{pmatrix} \tag{4}$$

and is diagonalized by a rotation in an angle β. We define $s_{\beta} = \sin\beta$, $c_{\beta} = \cos\beta$, and $t_{\beta} = \tan\beta$. $\mathbf{M}_A^2$ has a zero eigenvalue corresponding to the neutral Goldstone boson while its second eigenvalue is the mass of the physical CP-odd Higgs boson A,

$$m_A^2 = \frac{m_{12}^2}{s_{\beta}c_{\beta}} - \lambda_5 v^2 \,, \tag{5}$$

with $v^2 = v_1^2 + v_2^2$. The charged Higgs mass matrix is given by

$$\mathbf{M}_{\mathrm{H}^{\pm}}^2 = \\ \begin{pmatrix} m_{12}^2 t_{\beta} - \tfrac{1}{2}(\lambda_4 + \lambda_5)v^2 s_{\beta}^2 & -m_{12}^2 + \tfrac{1}{2}(\lambda_4 + \lambda_5)v^2 s_{\beta}c_{\beta} \\ -m_{12}^2 + \tfrac{1}{2}(\lambda_4 + \lambda_5)v^2 s_{\beta}c_{\beta} & m_{12}^2/t_{\beta} - \tfrac{1}{2}(\lambda_4 + \lambda_5)v^2 c_{\beta}^2 \end{pmatrix}, \tag{6}$$

which also is diagonalized by a rotation in an angle β. It has a zero eigenvalue corresponding to the charged Goldstone boson, and the charged Higgs mass is

$$m_{H^{\pm}}^2 = m_A^2 + \frac{1}{2}(\lambda_5 - \lambda_4)v^2 \,. \tag{7}$$

Here we see that the charged and the CP-odd Higgs masses are independent parameters, as opposed to supersymmetry, where the mass squared difference is equal to m_W^2 at tree level.

The neutral CP-even Higgs mass matrix is given by

$$\mathbf{M}_{H^0}^2 = \\ \begin{pmatrix} m_A^2 s_{\beta}^2 + \lambda_1 v^2 c_{\beta}^2 & -m_A^2 s_{\beta}c_{\beta} + (\lambda_3 + \lambda_4)v^2 s_{\beta}c_{\beta} \\ -m_A^2 s_{\beta}c_{\beta} + (\lambda_3 + \lambda_4)v^2 s_{\beta}c_{\beta} & m_A^2 c_{\beta}^2 + \lambda_2 v^2 s_{\beta}^2 \end{pmatrix} \tag{8}$$

and the two eigenvalues are the masses of the neutral CP-even Higgs bosons h and H. It is diagonalized by an angle α defined by

$$\sin 2\alpha =$$
$$\frac{\left[-m_A^2 + (\lambda_3 + \lambda_4)v^2\right] s_{2\beta}}{\sqrt{\left[m_A^2 c_{2\beta} - \lambda_1 v^2 c_\beta^2 + \lambda_2 v^2 s_\beta^2\right]^2 + \left[m_A^2 - (\lambda_3 + \lambda_4)v^2\right]^2 s_{2\beta}^2}} . \tag{9}$$
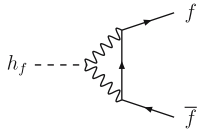
Fermiophobia is caused by imposing the mentioned discrete symmetry $\Phi_1 \to -\Phi_1$ which forbids Φ_1 coupling to the fermions. This model is usually called "Type I" [2]. However, fermiophobia is erased due to the mixing in the CP-even neutral Higgs mass matrix, which is diagonalized by the mixing angle α, when both CP-even eigenstates h^0 and H^0 acquire a coupling to the fermions.

The fermionic couplings of the lightest CP-even Higgs h^0 take the form $h^0 f\overline{f} \sim \cos\alpha/\sin\beta$, where f is any fermion. Small values of $\cos\alpha$ would strongly suppress the fermionic couplings, and in the limit $\cos\alpha \to 0$ the coupling $h^0 f\overline{f}$ would vanish at tree level, giving rise to fermiophobia. This is achieved if

$$m_A^2 = (\lambda_3 + \lambda_4)v^2 . \tag{10}$$

Despite this extra constraint, the parameters m_A, $m_{H^\pm}$ and $\tan\beta$ are still independent parameters in this model.

However, at the one-loop level, Higgs boson couplings to fermions receive contributions from loops involving vector bosons and other Higgs bosons,

$$\sim \frac{1}{16\pi^2}(gm_W)\left(\frac{g^2}{8}\right)m_f C_0(m_h^2, 0, 0; 0, m_W^2, m_W^2) ,$$

where we have naively estimated the contribution of the loop with the Passarino–Veltman function C_0. To get an order of magnitude of the correction we approximate $C_0 \sim 1/m_h^2$, as expected in the limit of large Higgs mass, and compare this correction with the tree-level vertex in the SM $g_{\phi^0 ff} \sim gm_f/2m_W$. We find

$$\frac{\Delta g_{hff}}{g_{\phi^0 ff}} \sim \frac{g^2}{64\pi^2}\left(\frac{m_W}{m_h}\right)^2 . \tag{11}$$

This estimation is also applicable if $m_h \lesssim m_W$ replacing m_h by m_W. This is a very small correction. Nevertheless, we note that the proper renormalization of the $\phi^0 f\overline{f}$ vertex involves a counterterm that has to be taken into account. It is conventional to define an extreme h_f in which all BRs to fermions are set to zero. This gives rise to benchmark BRs which are used in the current searches to set limits on m_{h_f}.

2.2 Higgs triplet models

Fermiophobia (or partial fermiophobia) can arise for scalar fields in isospin $I = 1$ triplet representations. Gauge invariance forbids any couplings of the triplet fields (χ) to quarks. For hypercharge $Y = 2$ triplets, the neutral Higgs field χ^0 can couple to leptons $(\nu\overline{\nu})$ via the following Yukawa type interaction [30]:[1]

$$h_{ij}\psi_{iL}^T Ci\tau_2, \Delta\psi_{jL} + \text{h.c.} \tag{12}$$

Here h_{ij} $(i, j = 1, 2, 3)$ is an arbitrary coupling, C is the Dirac charge conjugation operator, $\psi_{iL} = (\nu_i, l_i)_L^T$ is a left-handed lepton doublet, and Δ is a 2×2 representation of the $Y = 2$ complex triplet fields:

$$\Delta = \begin{pmatrix} \chi^+/\sqrt{2} & \chi^{++} \\ \chi^0 & -\chi^+/\sqrt{2} \end{pmatrix} . \tag{13}$$

The interaction described in (12) has the virtue of being able to provide neutrino masses and mixings consistent with current neutrino oscillation data *without* invoking a right-handed neutrino. If the real part of the neutral triplet field χ^{0r} acquires a vacuum expectation value (VEV) $\langle\chi^{0r}\rangle = b$, the following Majorana mass matrix (m_{ij}) for neutrinos is generated:

$$m_{ij} = \sqrt{2}h_{ij}b . \tag{14}$$

Neutrino oscillation data constrain the product $h_{ij}b$, while h_{ij} is constrained directly by lepton flavor violating processes involving μ and τ, e.g. $\mu \to e\gamma$, $\mu \to eee$ [31, 32]. Hence it is clear that χ^0 is partially fermiophobic, with a small coupling to neutrinos.

We will consider the Higgs triplet model (HTM) of [4, 5] in which a complex $Y = 2$ triplet (Δ) and a real $Y = 0$ triplet (ξ^+, ξ^0, ξ^-) are added to the SM Lagrangian. The HTM preserves $\rho = 1$ at tree level if the VEV's of both the neutral members are equal: $\langle\chi^0\rangle = \langle\xi^0\rangle = b$. Taking the VEV of the Higgs doublet $\langle\Phi^0\rangle = a$, one has the following expression for m_W:

$$m_W^2 = \frac{1}{4}g^2(a^2 + 8b^2) \equiv \frac{1}{4}g^2 v^2 \tag{15}$$

where $v^2 = 246^2\,\text{GeV}^2$. It is convenient to define a doublet–triplet mixing angle analogous to $\tan\beta$ in the 2HDM:

$$\sin\theta_H = \left[\frac{8b^2}{a^2 + 8b^2}\right]^{1/2} . \tag{16}$$

In the HTM the physical Higgs boson mass spectrum is as follows (in the notation of [33]):

$$H_5^{\pm\pm}, H_5^\pm, H_5^0, H_3^\pm, H_3^0, H_1^0, H_1^{0'} . \tag{17}$$

The first five scalars are mass eigenstates, while the latter two can mix in general; see below. H_1^0 plays the role of the

---

[1] Note that there is no such interaction for $Y = 0$ triplets, which are rendered fermiophobic as a consequence of gauge invariance.

SM Higgs boson and is composed of the real part of the neutral doublet field. The eigenstate $H_1^{0'}$ is entirely composed of triplet fields and is given by

$$H_1^{0'} = \frac{1}{\sqrt{3}} \left(\sqrt{2}\chi^{0r} + \xi^0 \right) . \tag{18}$$

From the theoretical point of view, the size of the triplet VEV b is only constrained by the requirement that the doublet VEV a is sufficiently large to allow for a perturbative top quark Yukawa coupling. However, experimental constraints on $\sin\theta_H$ can be obtained by considering the effect of $H_3^{\pm}$ on processes such as $b \to s\gamma$, $Z \to b\bar{b}$ and B–$\bar{B}$ mixing [34, 35]. Since $H_3^{\pm}$ has identical fermionic couplings to that of $H^{\pm}$ in the 2HDM (Model I) with the replacement $\cot\beta \to \tan\theta_H$, one can derive the bound $\sin\theta_H \leq 0.4$.

In (18) the χ^{0r} component in $H_1^{0'}$ couples to $\nu\bar{\nu}$ via the h_{ij} coupling. One can see from (14) that the decay $H_1^{0'} \to \gamma\gamma$, mediated by W loops proportional to b, will dominate over $H_1^{0'} \to \nu\bar{\nu}$ if b is of the order of a few GeV. Thus $H_1^{0'}$ is a candidate for a h_f, with BR($H_1^{0'} \to \gamma\gamma$) essentially equal to that of the benchmark h_f model. However, in general H_1^0 and $H_1^{0'}$ mix through the following mass matrix written in the $(H_1^0, H_1^{0'})$ basis [33]:

$$\mathcal{M} = \begin{pmatrix} 8c_H^2(\lambda_1+\lambda_3) & 2\sqrt{6}s_H c_H \lambda_3 \\ 2\sqrt{6}s_H c_H \lambda_3 & 3s_H^2(\lambda_2+\lambda_3) \end{pmatrix} v^2 . \tag{19}$$

Here λ_i are dimensionless quartic couplings in the Higgs potential and $s_H = \sin\theta_H$, $c_H = \cos\theta_H$. The assumption that the λ_i couplings are roughly the same order of magnitude together with the imposition of the bound $s_H < 0.4$ results in very small mixing [36]. Moreover, $H_1^{0'}$ would be the lightest Higgs boson in the HTM limit of small s_H, as stressed in [37]. In this paper we will study the production process $qq' \to H_3^{\pm} H_1^{0'}$, assuming that $H_1^{0'}$ is a fermiophobic Higgs with BRs equivalent to the benchmark h_f model.

2.3 Fermiophobic Higgs boson branching ratios

For the sake of illustration, we depict in Fig. 1 the branching ratios of a fermiophobic Higgs boson h_f into VV where V can be either a W, Z or γ. In this figure we assumed that the h_f couplings to fermions are absent and that $h_f \to \gamma\gamma$ is mediated solely by a W boson loop,
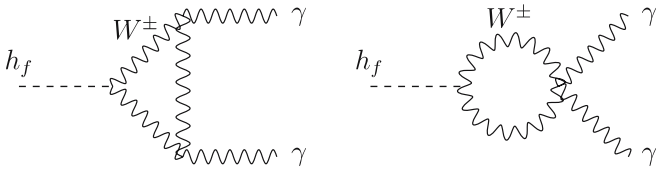
giving rise to the following h_f branching ratio into two photons:

$$\Gamma(h_f \to \gamma\gamma) = \frac{\alpha^2 g^2}{1024\pi^3} \frac{m_{h_f}^3}{m_W^2} |F_1 \cos\beta|^2 , \tag{20}$$

with $F_1 = F_1(\tau)$, $\tau = 4m_W^2/m_{h_f}^2$, a function given in [3]. We
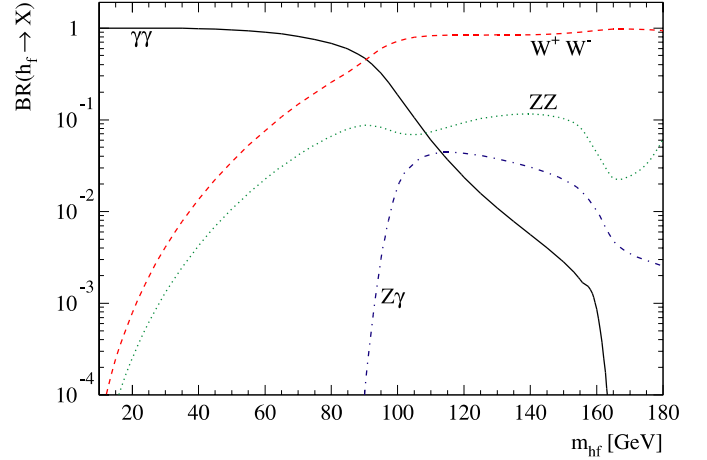

Fig. 1. Branching ratios of the largest decay modes of a fermiophobic Higgs boson assuming exact fermiophobia at tree level. The branching ratio into $\gamma\gamma$ equals the W^*W^* mode for $m_{h_f} \approx 90$ GeV and drops to 20% for $m_{h_f} = 100$ GeV

remind the reader that the $h_f WW$ coupling normalized to the SM $\phi_0 WW$ coupling satisfies $\sin(\beta-\alpha) \to \cos\beta$ in the fermiophobic limit.

This gives rise to benchmark BRs which are used in the ongoing searches to derive mass limits on m_{h_f}. In practice, $h_f \to \gamma\gamma$ can also be mediated by charged scalar loops: $H^{\pm}$ in the 2HDM [11, 12] and $H_3^{\pm}, H_5^{\pm}, H_5^{\pm\pm}$ in the HTM [38]. Although such contributions are suppressed relative to the W loops by a phase space factor, they can be important if the mixing angle suppression for the $h_f WW$ coupling ($\cos\beta$) is quite severe i.e. the scenario of interest in this paper. In our numerical analysis we will assume the benchmark BRs given in Fig. 1. One can see from the figure that the loop induced decay mode $h_f \to \gamma\gamma$ is dominant for $m_{h_f} \lesssim 95$ GeV and drops below 0.1% for h_f masses above 150 GeV. On the other hand, the decay channel $h_f \to W^*W^*$ dominates for $m_{h_f} \gtrsim 95$ GeV, being close to 100% until the threshold for h_f decay into two real Z's is reached.

2.4 The decay $H^{\pm} \to h_f W^*$

The experimental signature of the process $qq' \to H^{\pm} h_f$ depends on the decay modes of $H^{\pm}$. If $H^{\pm}$ decays to two fermions, then the signal would be of the type, $\gamma\gamma + X$, which is essentially the same as that assumed in the inclusive searches. However, crucial to our analysis is the fact that the decay $H^{\pm} \to h_f W^*$ may have a very large BR [27] in the 2HDM (Model I). This is because the decay width to the fermions ($H^{\pm} \to f'\bar{f}$) scales as $1/\tan^2\beta$. A similar behaviour occurs in the HTM [28] for the decay $H_3^{\pm} \to H_1^{0'} W^*$ with the replacement $1/\tan^2\beta \to \tan^2\theta_H$. Thus in the region of $\tan\beta > 10$ (or small $\sin\theta_H$) the fermionic decays of $H^{\pm}$ are depleted. This enables the decay $H^{\pm} \to h_f W^*$ ($H_3^{\pm} \to H_1^{0'} W^*$) to become the dominant channel *even if* the mass difference $m_{H^{\pm}} - m_{h_f}$ is much less than m_W. In Fig. 2 we show the branching ratios of the
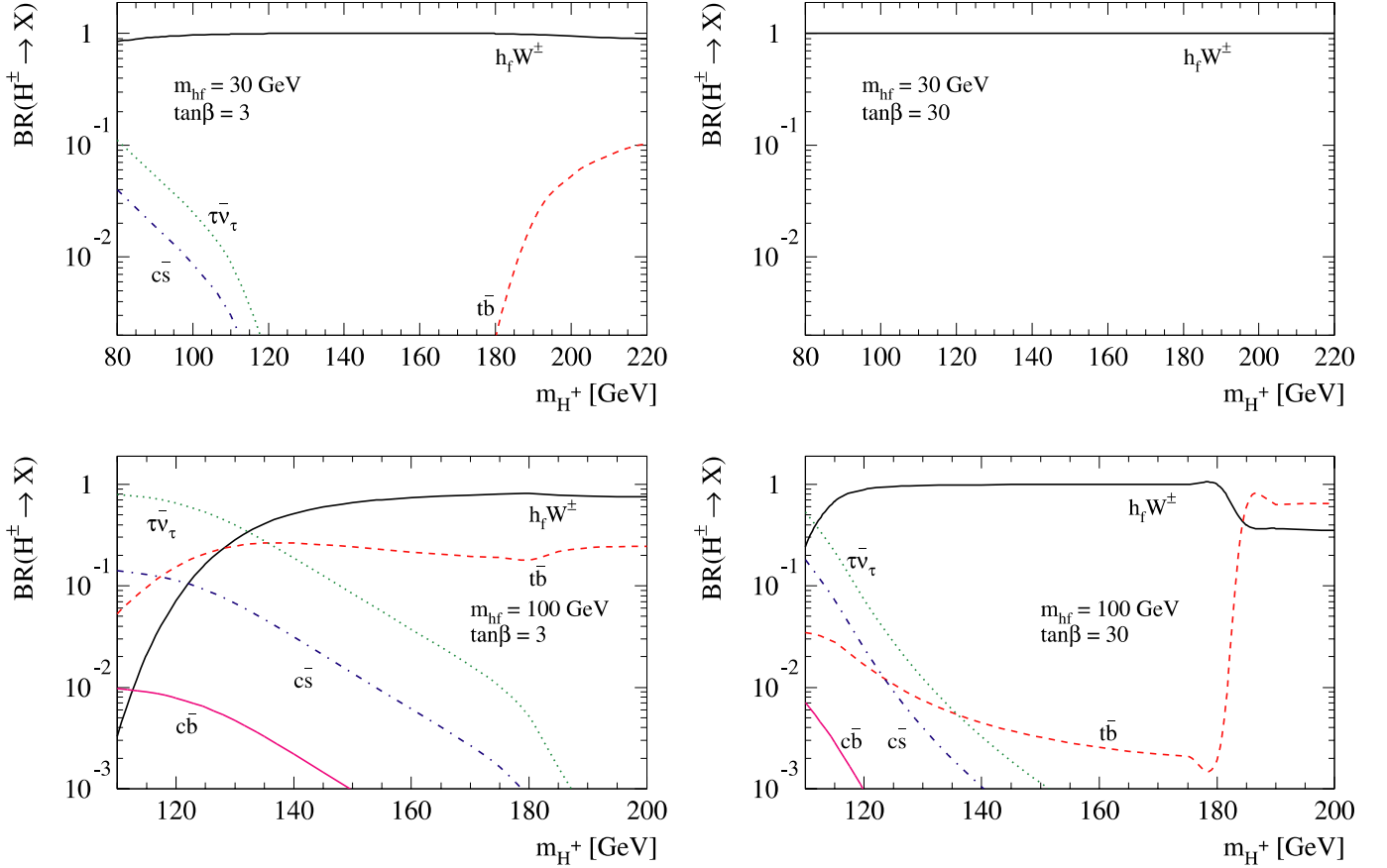
Fig. 2. The charged Higgs boson branching ratios into fermions $\tau\nu_\tau$ (*green/dotted*), tb (*red/dashed*), cs (*blue/dot-dashed*), and cb (*magenta/solid*), and W^*h_{f} (*black/solid*) as a function of the charged Higgs boson mass for two different $\tan\beta$ and fermiophobic Higgs mass values

charged Higgs boson into fermions and $h_{\mathrm{f}}W^*$ as a function of $M_{H^\pm}$ for several values of $\tan\beta$ and $m_{h_{\mathrm{f}}}$. From the right panels we see that in the large $\tan\beta$ regime the fermionic decays are indeed suppressed. Moreover, we also see that for light fermiophobic Higgs bosons, where a W boson can be produced on its mass shell, the decay $H^\pm \to W^\pm h_{\mathrm{f}}$ is essentially 100% for any $\tan\beta$. On the other hand, for heavier fermiophobic Higgs bosons, the fermionic decays can be the preferred decay channels mainly for small $\tan\beta$.

3 Phenomenology of h_{f} at hadron colliders

3.1 h_{f} production via the VVh_{f} coupling

Current searches at the Tevatron assume that production of h_{f} proceeds via the VVh_{f} coupling ($V = W, Z$) that originates from the kinetic part of the Lagrangian. Run I searches utilized the process $qq' \to Vh_{\mathrm{f}}$ giving a signature of a $\gamma\gamma$ and a vector boson [19, 20]. The preliminary Run II search is for inclusive $\gamma\gamma$ [24] and is therefore sensitive to both $qq' \to Vh_{\mathrm{f}}$ and the subdominant vector boson fusion $qq' \to h_{\mathrm{f}}qq$ [21]. Note that $gg \to h_{\mathrm{f}}$ via a fermion loop does not contribute to h_{f} production.

In the 2HDM (Model I) the strength of the VVh_{f} coupling relative to the SM coupling $VV\phi^0$ is given by

$$VVh_{\mathrm{f}} \propto \frac{1}{\sqrt{1+\tan^2\beta}} \,. \tag{21}$$

Hence the production mechanism $qq \to V^* \to Vh_{\mathrm{f}}$ can be rendered completely ineffective for $\tan\beta > 10$. In the HTM the fermiophobic Higgs boson has a coupling size relative to $VV\phi^0$ given by

$$VVH_1^{0'} \propto \frac{2\sqrt{2}}{\sqrt{3}} \, s_{\mathrm{H}} \,. \tag{22}$$

In direct analogy to the large $\tan\beta$ case of the 2HDM (Model I), a small s_{H} would suppress the coupling $VVH_1^{0'}$ and consequently deplete the $h_{\mathrm{f}}V$ production. Hence it is of concern to consider other production mechanisms which are unsuppressed in the above scenario.

3.2 Associated h_{f} production with $H^\pm$ and the multi-photon signature

The production mechanism $qq' \to H^\pm h_{\mathrm{f}}$ is complementary to that of $qq' \to Vh_{\mathrm{f}}$. This can be seen immediately from

the explicit expressions for the couplings. In the 2HDM (Model I) one has

$$VH^{\pm}h_{\mathrm{f}} \propto \frac{\tan\beta}{\sqrt{1+\tan^2\beta}} \,, \qquad (23)$$

while in the HTM

$$VH^{\pm}H_1^{0'} \propto \frac{2\sqrt{2}}{\sqrt{3}} \, c_{\mathrm{H}} \,. \qquad (24)$$

Hence the above couplings are unsuppressed in the region of the parameter space where the standard production mechanism $qq' \to Vh_{\mathrm{f}}$ becomes ineffective. The larger coefficient for the $VH_3^{\pm}H_1^{0'}$ coupling is a consequence of the quantum number (I, Y) assignments in the HTM.

To date complementary mechanisms have not been considered in the direct fermiophobic Higgs searches at the Tevatron. As emphasized in [25, 26] a more complete search strategy for h_{f} at hadron colliders must include such production processes in order to probe the scenario of fermiophobic Higgs bosons with a suppressed coupling $h_{\mathrm{f}}VV$. In the HTM one expects $H_1^{0'}$ to be the lightest Higgs boson for small $\sin\theta_{\mathrm{H}}$, which further motivates a search in the complementary channel $qq' \to H_3^{\pm}H_1^{0'}$.

The experimental signature arising from the complementary mechanism $qq' \to H^{\pm}h_{\mathrm{f}}$ depends on the $H^{\pm}$ decay channel. In a large fraction of the parameter space where the complementary mechanism $qq' \to H^{\pm}h_{\mathrm{f}}$ is important, the $H^{\pm}$ decay is dominated by $H^{\pm} \to h_{\mathrm{f}}W^*$. Consequently, this scenario would give rise to double h_{f} production, with subsequent decay of $h_{\mathrm{f}}h_{\mathrm{f}} \to \gamma\gamma\gamma\gamma, VV\gamma\gamma$ and $VVVV$. For light h_{f} ($m_{h_{\mathrm{f}}} \lesssim 90\,\mathrm{GeV}$), the signal $\gamma\gamma\gamma\gamma$ would dominate, as discussed in [27] at LEP, in [25] for the Tevatron Run II and [26] at the LHC and the Linear Collider. More specifically, the multi-photon signature arises in the portion of the parameters space where $m_{h_{\mathrm{f}}} \lesssim 90\,\mathrm{GeV}$, $m_{H^{\pm}} \lesssim 200\,\mathrm{GeV}$, and $\tan\beta > 1$ in the 2HDM Model I framework. In that region, $\mathrm{BR}(h_{\mathrm{f}} \to \gamma\gamma) \sim 1$ and $\mathrm{BR}(H^{\pm} \to h_{\mathrm{f}}W^{*\pm}) \sim 1$ as well, leading to a $4\gamma + $ leptons or jets signature.

As explained in [25], processes other than $qq' \to H^{\pm}h_{\mathrm{f}}$ could give rise to a $4\gamma + X$ signal. One such mechanism is $q\bar{q} \to A^0h_{\mathrm{f}}$, where A^0 is the heavy neutral pseudoscalar decaying $A^0 \to h_{\mathrm{f}}Z^*$. However, LEP already searched for $e^+e^- \to h_{\mathrm{f}}A^0$ and set the bound $m_{h_{\mathrm{f}}} + m_A > 160\,\mathrm{GeV}$ [13]. Thus any contribution from $qq \to A^0h_{\mathrm{f}}$ will be phase space suppressed relative to that originating from $qq' \to H^{\pm}h_{\mathrm{f}}$. A similar argument applies to the production of a pair of charged Higgs bosons and its subsequent decay into $h_{\mathrm{f}}V^*$ pairs, i.e. $q\bar{q} \to Z^*, \gamma^* \to H^+H^- \to h_{\mathrm{f}}h_{\mathrm{f}}W^+W^-$ which is phase space suppressed at Tevatron energies ($2m_{H^{\pm}} > 180\,\mathrm{GeV}$ from direct $H^{\pm}$ searches). In the minimal supersymmetric model the total rates for H^+H^- production are enhanced in the large $\tan\beta$ regime through the Yukawa couplings of Higgs bosons to bottom quarks [39], however in the 2HDM (Model I) and HTM, these Yukawa couplings are suppressed. The LHC would probably have much better prospects in these additional channels if all the above pair production mechanisms were combined with the $H^{\pm}h_{\mathrm{f}}$ associated production in a fully inclusive multi-photon search. Since our analysis for the Tevatron we will focus on $qq' \to H^{\pm}h_{\mathrm{f}}$, which provides the best search potential for the very light h_{f} region because the phase space constraint ($m_{H^{\pm}} + m_{h_{\mathrm{f}}} > 100\,\mathrm{GeV}$) is the least restrictive of the Higgs pair production mechanisms.

4 Multi-photon signal analyses

We now present our analysis for the inclusive production of multi-photon final states which may or may not be accompanied by extra leptons and/or jets, i.e. the reaction

$$p\bar{p} \to h_{\mathrm{f}}H^{\pm} \to h_{\mathrm{f}}h_{\mathrm{f}}W^{\pm} \to \gamma\gamma\gamma\gamma + X \,,$$

at the Tevatron Run II. We focus our attention on two inclusive final states; (i) at least three photons ($> 3\gamma$) and (ii) four photons (4γ). Only the "1-prong" tau lepton decays were considered.
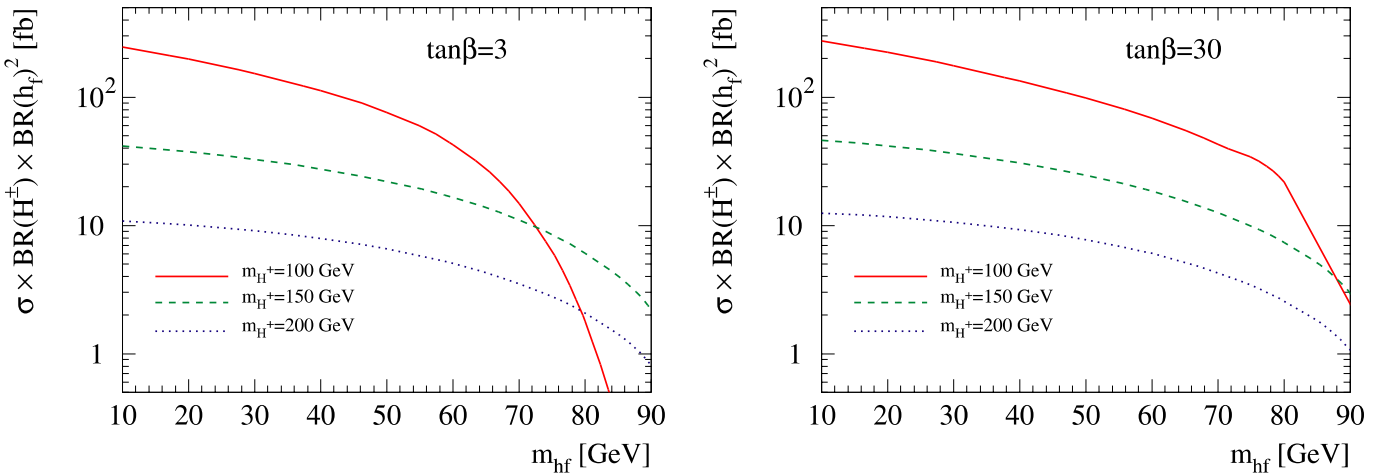

Fig. 3. Total production cross sections times branching ratios of $h_{\mathrm{f}} \to \gamma\gamma$ and $H^{\pm} \to W^{\pm}h_{\mathrm{f}}$ for $p\bar{p} \to h_{\mathrm{f}}H^{\pm} \to h_{\mathrm{f}}h_{\mathrm{f}} + W^{\pm} \to \gamma\gamma\gamma\gamma + W^{\pm}$ before cuts at the Tevatron Run II in femtobarns. The values of $\tan\beta$ and $m_{H^{\pm}}$ are as indicated in the figure
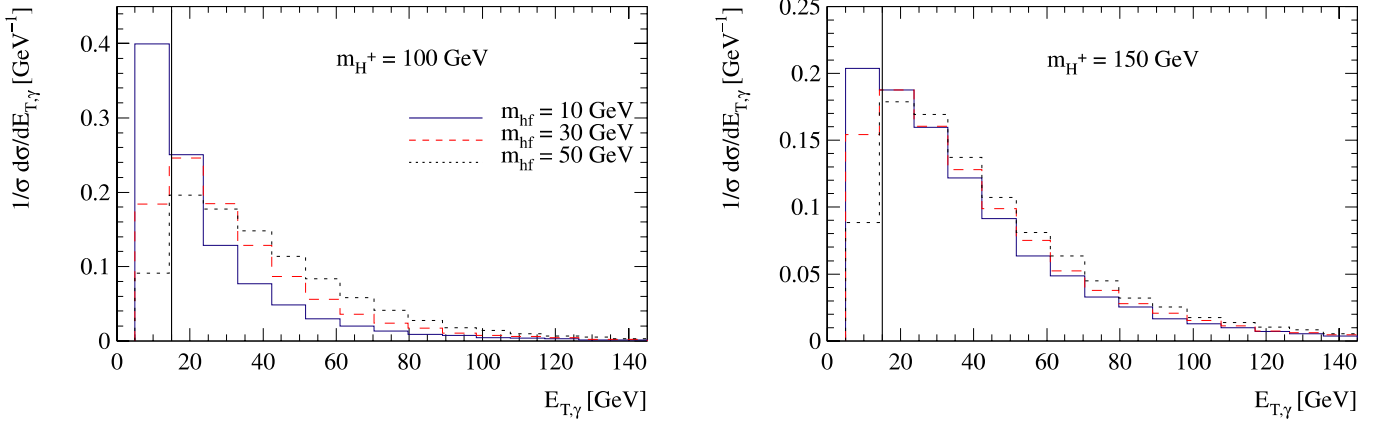
Fig. 4. Normalized transverse energy distributions (in GeV) of photons for two different charged Higgs boson masses and three different fermiophobic Higgs masses. The *vertical solid lines* indicate the E_{T}^{γ} cut in (25)
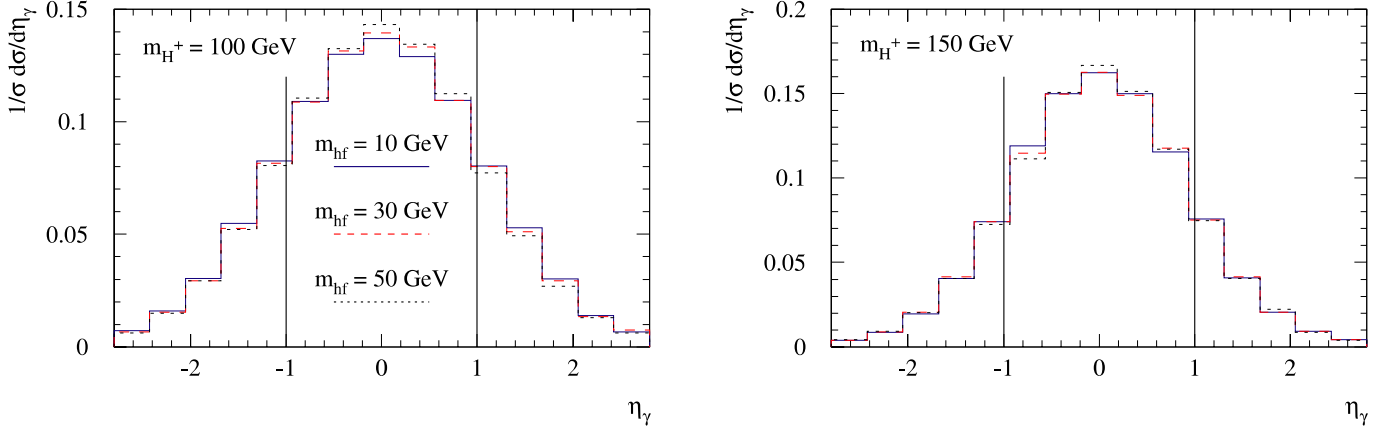

Fig. 5. Normalized rapidity distributions of photons for two different charged Higgs boson masses and three different fermiophobic Higgs masses. The *vertical solid lines* indicate the η_γ cut of (25)

In our analysis we evaluated the signal and standard model backgrounds at the parton level. We calculated the full matrix elements using the helicity formalism with the help of Madevent [40, 41]. We employed CTEQ6L1 parton distributions functions [42] evaluated at the factorization scale $Q_{\mathrm{F}} = \sqrt{\hat{s}}$, where $\sqrt{\hat{s}}$ is the partonic center-of-mass energy. Although QCD corrections increase the tree-level cross section by a factor of around 1.3 [43], we shall present results using the tree-level cross sections only. Moreover we included momenta smearing effects as given in [19, 44–46] and a detection efficiency of 85% per photon.

We present in Fig. 3 the total signal cross section times the branching ratios of $H^{\pm} \to h_{\mathrm{f}} W^{\pm}$ and $h_{\mathrm{f}} \to \gamma\gamma$ for the complementary process $q q' \to H^{\pm} h_{\mathrm{f}}$; these results were obtained without cuts and detection efficiencies. In the left (right) panel we present the 4γ production cross section before cuts as a function of $m_{h_{\mathrm{f}}}$ for three different values of $m_{H^{\pm}}$ and $\tan\beta = 3$ (30). In the left panel, where $\tan\beta = 3$, the upper curve ($m_{H^{\pm}} = 100\,\mathrm{GeV}$) shows the strongest effect of the phase space suppression of the decay $H^{\pm} \to W^* h_{\mathrm{f}}$ for $m_{h_{\mathrm{f}}} \gtrsim 60\,\mathrm{GeV}$. This cross section reduction can be partially compensated by the increase in $\tan\beta$ as shown in

the right panel. From the figure it is evident that this process will produce a large number of events before cuts over a large fraction of the parameter space.

Potential SM backgrounds for the multi-photon signature of fermiophobic Higgs bosons are (i) the three and four photon production $p\bar{p} \to \gamma\gamma\gamma(\gamma)$, (ii) three photons and a W production $p\bar{p} \to \gamma\gamma\gamma W$, and (iii) the associated production of two or three photons and a jet where the latter is misidentified as a photon $p\bar{p} \to \gamma\gamma(\gamma)j(\to \gamma + X)$.

We verified that after cuts and taking into account a $P(j \to \gamma) = 4 \times 10^{-4}$ [44–46] photon misidentification probability the total SM background amounts to 3.8 events for an integrated luminosity of $2\,\mathrm{fb}^{-1}$. Therefore the complementary process for the fermiophobic Higgs search has the great advantage of being extremely clean for a large portion of the 2HDM and HTM parameter space.[2] In contrast, the ongoing search for inclusive $\gamma\gamma + X$ [24] suffers from a sizeable background originating from QCD jets faking photons. For the exclusive channel ($\gamma\gamma + V$) the

---

[2] After completion of this work, preliminary results for a search in the triphoton channel have been released by the CDF Collaboration [47].
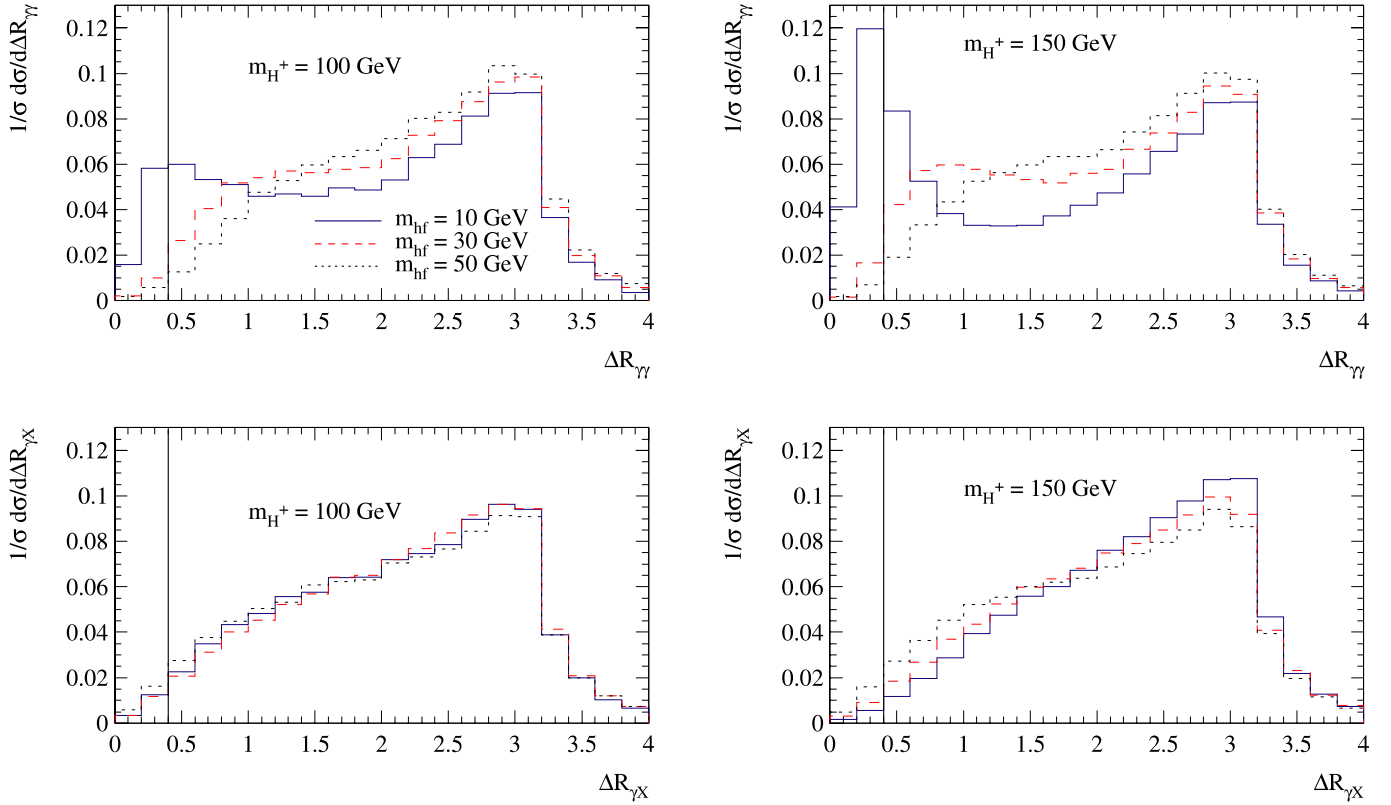
Fig. 6. Normalized cone variable distributions between two photons (*upper panels*), a photon and a charged particle or jet (*lower panels*) for the same parameter used in Fig. 4. The *vertical solid lines* indicate the ΔR cuts in (26)
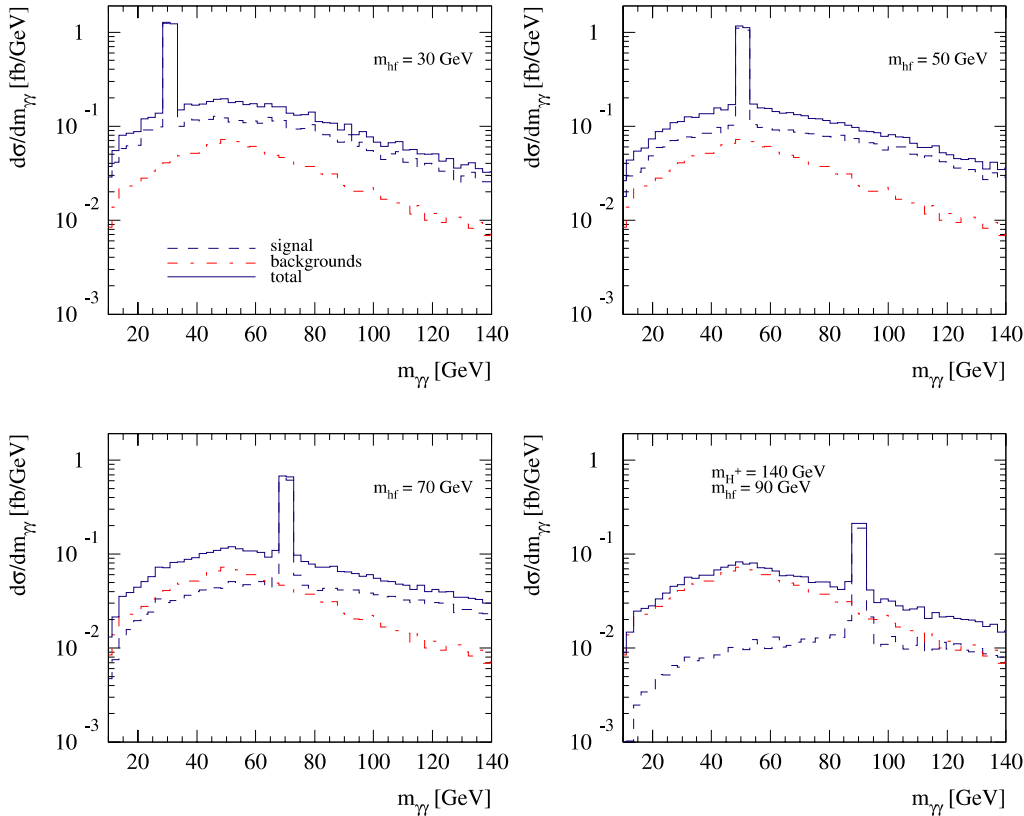

Fig. 7. The photon–photon invariant mass spectrum for $m_{H^\pm} = 150$ GeV, $m_{h_f} = 30$, 50, 70 GeV, and $m_{H^\pm} = 140$ GeV, $m_{h_f} = 90$ GeV at the *upper left, upper right, bottom left*, and *bottom right* panels, respectively. Also shown are the sum of all backgrounds consisting of $3\gamma + X$ final states. In these plots we entered the invariant mass of all photon pairs' possible combinations. In all cases we set $\tan\beta = 30$

background is considerably smaller but still not negligible [19, 20].

4.1 Searches at the Tevatron Run II

The multi-photon topology is privileged concerning the level of background, which is small in the SM after mild cuts. Consequently, we imposed a minimum set of cuts on the final state particles, in order to guarantee their identification and isolation. Further studies could optimize the search strategy. We required the events to possess central photons with enough transverse energy to assure their proper identification

$$E_T^\gamma > 15\,\text{GeV} \quad , \quad |\eta^\gamma| < 1.0 \,, \tag{25}$$

and isolated from the other particles in the final state ($X =$ charged lepton or jet) with a transverse energy in excess of 5 GeV

$$\Delta R_{\gamma\gamma} > 0.4 \quad , \quad \Delta R_{\gamma X} > 0.4 \,. \tag{26}$$

Notice that the high p_T central photons is enough to guarantee the trigger of these events [44–46]. These cuts are very effective against the backgrounds from continuous $\gamma\gamma\gamma + X$ production which occur mainly through photon and gluon bremsstrahlung emission from initial and/or final state quarks, and gluon splitting to collinear quarks. We have checked that $4\gamma + X$ topologies give a negligible contribution after imposing the cuts.

In order to understand the effect of these cuts on the signal we studied some kinematical distributions. We present in Fig. 4 the normalized transverse energy distribution of the final state photons for several values of Higgs masses and $\tan\beta = 30$. As one can see, the E_T^γ spectrum peaks around $\lesssim m_{h_f}/2$ and the spectrum at low E_T^γ decreases as the fermiophobic Higgs becomes heavier. We can also learn that the E_T^γ distribution becomes harder as the charged Higgs mass increases. Thus, the transverse energy cut in (25) attenuates more the light fermiophobic Higgs signal.

Figure 5 contains the photon rapidity distribution for the same parameters as used in Fig. 4. The rapidity distribution of the photons stemming from the fermiophobic Higgs decay peaks around zero. However, there is a sizeable contribution from high rapidity photons. For heavier charged Higgs bosons the rapidity distribution is more central. The hardest cut that we applied is the requirement that the absolute value of the photon rapidity be smaller than unity, and its effect is rather insensitive to the neutral Higgs mass. On the other hand, the separation cuts in (26) have little effect on the signal cross section as shown in Fig. 6, with perhaps the exception of very small fermiophobic Higgs masses. Notice that we did not introduce any cut on the photon–photon invariant masses. Certainly if a signal is observed the photon pair invariant mass will display a clear peak at m_{h_f} even after adding all the possible photon pair combinations and backgrounds; see Fig. 7.

We display in Fig. 8 the region in the plane $m_{H^\pm} \otimes m_{h_f}$ where at least a 3σ signal can be observed, exhibiting three or more photons, in the framework of the 2HDM Model I

for an integrated luminosity of $2\,\text{fb}^{-1}$. The statistical significance σ is defined by $\sigma = S/\sqrt{B}$, where $S(B)$ is the number of signal (background) events after applying cuts and efficiency factors.

A few comments are in order. First of all, the expected number of events diminishes for small h_f masses since fewer events pass the E_T^γ cut in (25) as can be seen from Fig. 4. Secondly, the shape of the region presenting at least 3σ (5σ or 10σ) significance in the large h_f mass region is the result of a competition between the phase space suppression of the cross section as $m_{H^\pm}$ increases for fixed m_{h_f} and the growth of the $H^\pm \to W^\pm h_f$ branching ratio; see Fig. 2. Furthermore, for a fixed number of events, the optimum reach in $m_{H^\pm}$ takes place for $m_{h_f} \simeq 30$–$40\,\text{GeV}$. This is a consequence of the combined effects of cuts and phase space suppression, as we have already discussed.
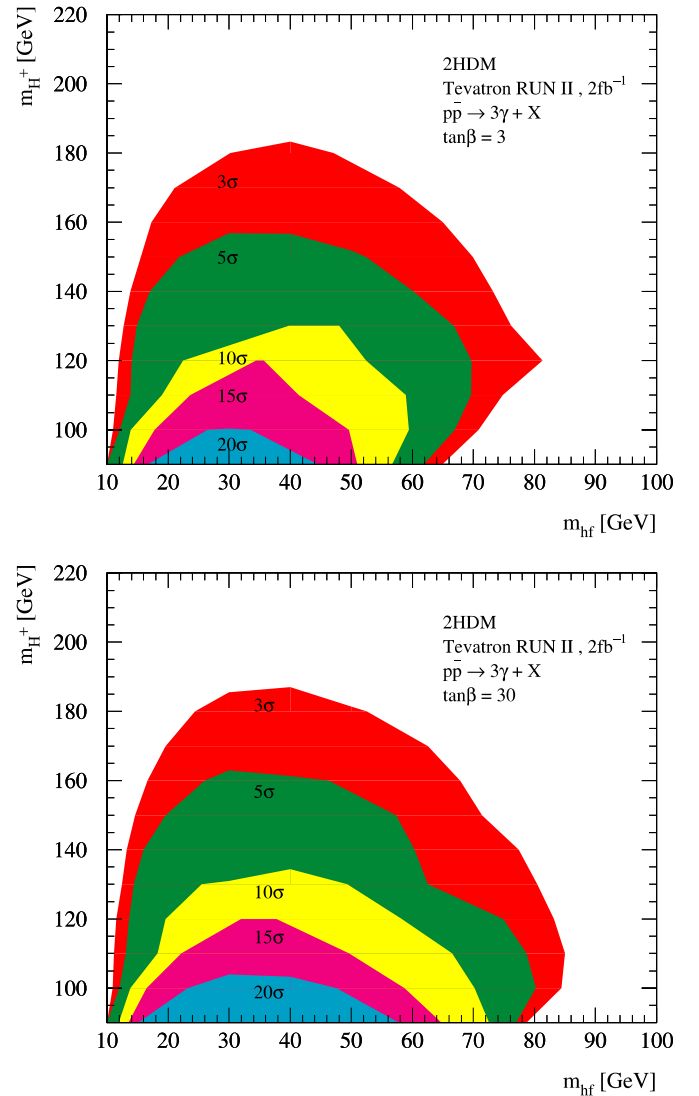

Fig. 8. Expected signal statistical significance presenting three or more photons in the $m_{H^\pm} \otimes m_{h_f}$ plane assuming an integrated luminosity of $2\,\text{fb}^{-1}$ at the Tevatron RUN II. We assumed the 2HDM Model I and took $\tan\beta = 3$ (30) in the *upper* (*lower*) *panel*

As one can see from the upper panel in Fig. 8, even in the low $\tan\beta$ region the reach of the Tevatron RUN II is quite impressive in this scenario. If no events were observed above the backgrounds at RUN II, a large fraction of the $m_{H^\pm}\otimes m_{h_f}$ plane would be excluded at the 3σ level. The situation improves slightly for larger $\tan\beta$ as can be seen from the lower panel of Fig. 8. Importantly, the expected number of events is rather large in the region $m_{h_f}\lesssim 70$ GeV and $m_{H^\pm}\lesssim 150$ GeV, so that it will be possible to reconstruct the h_f mass from the photon–photon invariant mass distribution; see Fig. 7. In Fig. 9 we sho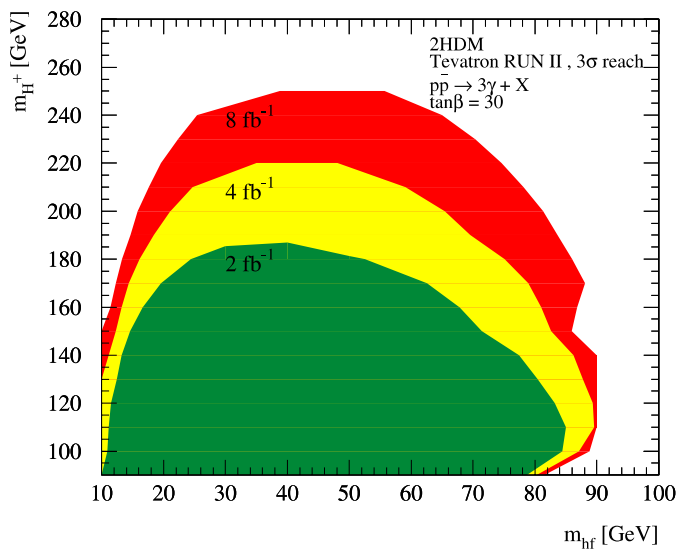w the region in the $m_{H^\pm}\otimes m_{h_f}$ plane giving rise to a statistical significance $> 3\sigma$ for integrated luminosities of 2,4 and 8 fb^{-1} for the case of $\tan\beta = 30$. One can see that the discovery reach can be considerably improved if cases with > 2 fb^{-1} are accumulated; e.g. for $m_{h_f} = 30$ GeV the 3σ evidence extends from $m_{H^\pm} = 180$ GeV to $m_{H^\pm} = 240$ GeV as the luminosity increases from 2 fb^{-1} to 8 fb^{-1}.

For comparison, we present in Fig. 10 the expected signal significance of events containing three or more photons after cuts for the HTM. In our numerical analysis we take $c_H = 1$ as a benchmark value, and the signal significance for other values of c_H can be obtained by simply rescaling the displayed numbers. From the bound $s_H < 0.4$ one obtains $c_H > 0.9$. In the exact $c_H = 1$ limit (i.e. triplet VEV $b = 0$) the neutrinos would not receive a mass at tree level (see (14)). Extremely small values, $s_H < 10^{-9}$, would require non-perturbative values of h_{ij} to generate realistic neutrino masses. We are interested in the interval $0.9 < c_H < 0.99$ (corresponding to GeV scale triplet VEV) in which $H_1^{0'}$ decays primarily to photons in the detector, and neutrino mass is generated with a very small $h_{ij} \sim 10^{-10}$.

It is clear that a larger region of the $m_{h_f}\otimes m_{H^\pm}$ parameter space can be probed in the HTM than in the 2HDM. In fact, at the 3σ level RUN II will be able to exclude Higgs masses up to $m_{H^\pm}\lesssim 240$ GeV or $m_{h_f}\lesssim 100$ GeV. In
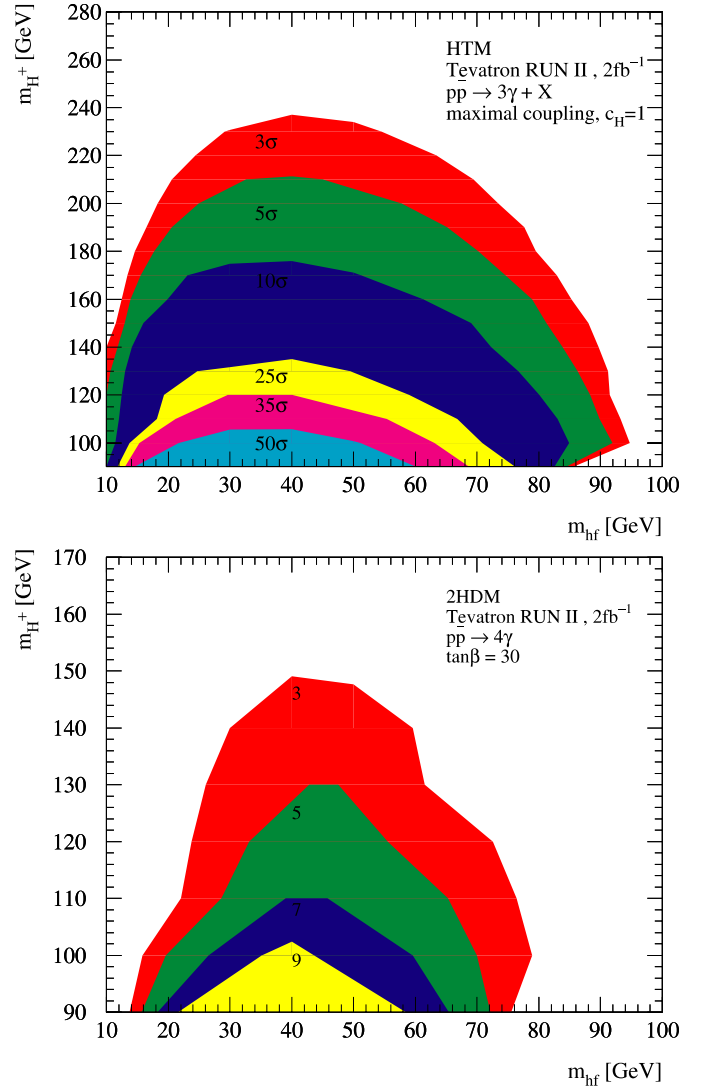

Fig. 10. In the *upper panel* we display the expected signal statistical significance containing three or more photons in the $m_{H^\pm}\otimes m_{h_f}$ plane in the HTM framework, assuming an integrated luminosity of 2 fb^{-1} at the Tevatron RUN II. In the *lower panel* we display the expected number of events presenting four photons in the $m_{H^\pm}\otimes m_{h_f}$ plane for the 2HDM Model I and assuming $\tan\beta = 30$

order to understand the signal suppression if one requires an inclusive state containing four photons to pass our cuts, we present in Fig. 10 lower panel the expected number of events for the 2HDM, assuming $\tan\beta = 30$ and an integrated luminosity of 2 fb^{-1}. As expected, not only the reach in $m_{H^\pm}$ gets reduced to $m_{H^\pm}\lesssim 150$ GeV at 95% C.L., but also the low and high h_f mass regions become substantially depleted.

5 Conclusions

Fig. 9. The region in the $m_{H^\pm}\otimes m_{h_f}$ plane giving rise to a statistical significance $> 3\sigma$ for integrated luminosities of 2,4 and 8 fb^{-1}. We take $\tan\beta = 30$ and assume the 2HDM Model I

Higgs bosons with very suppressed couplings to fermions (h_f) can arise in various extensions of the standard model,

such as the two Higgs doublet model (2HDM) Type I or Higgs triplet model (HTM). Their conventional production mechanism at hadron colliders $qq' \to W^{\pm}h_{\mathrm{f}}$ can be severely suppressed by either a large $\tan\beta$ or a small triplet vacuum expectation value. In this scenario the complementary channel $p\bar{p} \to H^{\pm}h_{\mathrm{f}}$ is maximal and provides an alternative production mechanism. We studied the reaction $qq' \to H^{\pm}h_{\mathrm{f}}$ followed by the potentially important decay $H^{\pm} \to h_{\mathrm{f}}W^*$. We performed a Monte Carlo simulation of the detection prospects for a light h_{f} where the branching ratio into photon pairs is dominant, which gives rise to multi-photon signatures with very low SM background. We showed that if a signal containing at least three photons is not seen at the Tevatron RUN II, then a large portion of the $m_{H^{\pm}}$ versus $m_{h_{\mathrm{f}}}$ plane can be excluded both in the small and large $\tan\beta$ regimes of the 2HDM. Conversely, if a signal *were* observed then > 50 events are expected for a light $H^{\pm}$ and h_{f}, which would allow for further detailed phenomenological studies.

References

1. T.J. Weiler, Proceedings of the 8th Vanderbilt Int. Conf. on High Energy Physics (Nashville, TN, October 8–10, 1987), ed. by J. Brau, R. Panvini (World Scientific, Singapore, 1988), p. 219
2. H.E. Haber, G.L. Kane, T. Sterling, Nucl. Phys. B **161**, 493 (1979)
3. J.F. Gunion, H.E. Haber, G.L. Kane, S. Dawson, The Higgs Hunter's Guide (Addison–Wesley, Reading, MA, 1989)
4. H. Georgi, M. Machacek, Nucl. Phys. B **262**, 463 (1985)
5. M.S. Chanowitz, M. Golden, Phys. Lett. B **165**, 105 (1985)
6. A. Stange, W.J. Marciano, S. Willenbrock, Phys. Rev. D **49**, 1354 (1994)
7. M.A. Diaz, T.J. Weiler, arXiv:hep-ph/9401259
8. V.D. Barger, N.G. Deshpande, J.L. Hewett, T.G. Rizzo, arXiv:hep-ph/9211234, in Argonne 1993, Physics at current accelerators and supercolliders* 437–442
9. H. Pois, T.J. Weiler, T.C. Yuan, Phys. Rev. D **47**, 3886 (1993)
10. A.G. Akeroyd, Phys. Lett. B **368**, 89 (1996)
11. A. Barroso, L. Brucher, R. Santos, Phys. Rev. D **60**, 035005 (1999)
12. L. Brucher, R. Santos, Eur. Phys. J. C **12**, 87 (2000)
13. OPAL Collaboration, G. Abbiendi et al., Phys. Lett. B **544**, 44 (2002)
14. DELPHI Collaboration, P. Abreu et al., Phys. Lett. B **507**, 89 (2001)
15. DELPHI Collaboration, P. Abreu et al., Eur. Phys. J. C **35**, 313 (2004)
16. ALEPH Collaboration, A. Heister et al., Phys. Lett. B **544**, 16 (2002)
17. L3 Collaboration, P. Achard et al., Phys. Lett. B **534**, 28 (2002)
18. L3 Collaboration, P. Achard et al., Phys. Lett. B **568**, 191 (2003)
19. DØ Collaboration, B. Abbott et al., Phys. Rev. Lett. **82**, 2244 (1999)
20. CDF Collaboration, T. Affolder et al., Phys. Rev. D **64**, 092002 (2001)
21. S. Mrenna, J. Wells, Phys. Rev. D **63**, 015006 (2001)
22. D0 Collaboration, V.M. Abazov et al., arXiv:hep-ex/0508054
23. G. Landsberg, K.T. Matchev, Phys. Rev. D **62**, 035004 (2000)
24. D0 Collaboration, A. Melnitchouk et al., Int. J. Mod. Phys. A **20**, 3305 (2005)
25. A.G. Akeroyd, M.A. Diaz, Phys. Rev. D **67**, 095007 (2003)
26. A.G. Akeroyd, M.A. Diaz, F.J. Pacheco, Phys. Rev. D **70**, 075002 (2004)
27. A.G. Akeroyd, Nucl. Phys. B **544**, 557 (1999)
28. A.G. Akeroyd, Phys. Lett. B **442**, 335 (1998)
29. J.F. Gunion, H.E. Haber, arXiv:hep-ph/0506227
30. J. Schechter, J.W.F. Valle, Phys. Rev. D **22**, 2227 (1980)
31. F. Cuypers, S. Davidson, Eur. Phys. J. C **2**, 503 (1998)
32. Y. Kuno, Y. Okada, Rev. Mod. Phys. **73**, 151 (2001)
33. J.F. Gunion, R. Vega, J. Wudka, Phys. Rev. D **42**, 1673 (1990)
34. A. Kundu, B. Mukhopadhyaya, Int. J. Mod. Phys. A **11**, 5221 (1996)
35. H.E. Haber, H.E. Logan, Phys. Rev. D **62**, 015011 (2000)
36. A.G. Akeroyd, Phys. Lett. B **353**, 519 (1995)
37. P. Bamert, Z. Kunszt, Phys. Lett. B **306**, 335 (1993)
38. J.F. Gunion, R. Vega, J. Wudka, Phys. Rev. D **43**, 2322 (1991)
39. A. Alves, T. Plehn, Phys. Rev. D **71**, 115014 (2005)
40. F. Maltoni, T. Stelzer, JHEP **0302**, 027 (2003)
41. T. Stelzer, W.F. Long, Phys. Commun. **81**, 357 (1994)
42. J. Pumplin, D.R. Stump, J. Huston, H.L. Lai, P. Nadolsky, W.K. Tung, JHEP **0207**, 012 (2002)
43. S. Dawson, S. Dittmaier, M. Spira, Phys. Rev. D **58**, 115012 (1998)
44. CDF Collaboration, A. Gajjar, arXiv:hep-ex/0505046
45. D0 Collaboration, V.M. Abazov et al., Phys. Rev. D **71**, 091108 (2005)
46. A. Melnitchouk, Ph.D. Thesis, FERMILAB-THESIS-2003-23 (2003)
47. http://www.cdf.fnal.gov/physics/exotic/r2a/20060223.diphotonPlusX/